Proceedings XII GEOINFO, November 27-29, 2011, Campos do Jordão, Brazil. p 85-96.

A Susceptible-Infected Model for Exploring the Effects of Neighborhood Structures on Epidemic Processes – A Segregation Analysis

Leonardo Bacelar Lima Santos[1], **Raian Vargas Maretto**[1], **Líliam César de Castro Medeiros**[1], **Flávia da Fonseca Feitosa**[1], **Antônio Miguel Vieira Monteiro**[1]

[1]Instituto Nacional de Pesquisas Espaciais – São José dos Campos, SP, Brasil

{santoslbl,raian,lccastro,flavia,miguel}@dpi.inpe.br

Abstract. *This work explores and analyzes the effects of neighborhood structures on disease spreading in a compartmental epidemic CA-model. The main goal is to investigate how different neighborhood configurations are able to affect the spatial and temporal distribution of infected and susceptible individuals and the chance of having members from these different groups interacting with each other. It uses the idea of "activity-space neighborhood", which extends traditional contiguity-based neighborhoods to capture interactions beyond those established in a residential environment. To depict the spatial distribution of infected and susceptible individuals along the simulation steps, we introduce the use of spatial segregation indices, traditionally adopted in urban studies, to an epidemiological context.*

1. Introduction and Motivation

Over the last decades, studies on epidemiology have recognized the importance of adopting a systemic view of epidemic processes. However, most of these approaches are based on ordinary differential equations or statistical models [19, 5, 26], which are unable to explore spatially-explicit patterns and interactions that are relevant to understand the dynamics of disease transmission.

To overcome these limitations, many studies have started using Cellular Automata (CA) models [35, 32] to obtain new insights on how epidemic processes evolve in time and space [22, 18, 16, 30, 33, 24]. Cellular automata are self-reproductive dynamic systems, where time and space are discretized [29]. They are composed of a lattice of cells, called cellular space, each one with a pattern of local connections to other cells, and subjected to given boundary conditions [33, 27]. Each cell can assume a state, among a enumerable set of states, which can change at every time-step according to local transition rules (deterministic or stochastic) based on the states of the cell and possibly of its neighbors. CA-based models have a long tradition in modeling and simulation of complex spatial phenomena, and its potential has been widely recognized in several fields of study [28, 1, 6, 34, 7].

In CA models, the concept of *neighborhoods* is a key component, since it determines how the elements that build up the model interact [14]. To say that two cells are neighbors means that one is exerting some sort of influence over the state (spatial, temporal and/or behavioral) of the other. Thus, it is an essential aspect to represent interactions between individuals in a society.

This paper investigates the effects of neighborhood structures on disease spreading by using a susceptible-infected (SI) epidemics CA-model. Despite its simplicity, the SI model can be used for early detection of infections diseases outbreaks [25] and has the advantage of being easily extended to models that accommodate additional categories [20], such as the susceptible-infected-susceptible (SIS) model – commonly used to represent bacterial infections –, the susceptible-infected-recovered (SIR) model – usually applied to viral infections –, or others epidemiological compartmental models [15]. The SI model can be also applied to problems of other nature, called general epidemic process, as forest fire propagation [2, 3] or the spread of information on a society [31].

This work dedicates particular attention to the spatial distribution of infected and susceptible individuals. Its main goal is to investigate how different neighborhood configurations are able to affect the spatial and temporal distribution of infected and susceptible people and the chance of having members from these different groups interacting with each other. It introduces the idea of "activity-space neighborhood", which extends traditional contiguity-based neighborhoods (e.g., Moore or Von Neumann) to capture not only interactions established in a residential environment, but also those resulting from other daily activities, such as work or school.

In addition, this study explores how the initial distribution of infected individuals influences the spatiotemporal patterns of disease spread. To depict the spatial distribution of infected and susceptible individuals along the simulation steps, we introduce the use of spatial segregation indices, traditionally adopted in urban studies, to an epidemiological context. Global and local spatial segregation indices are computed: while global indices express the segregation state for the city as a whole, local indices are able to depict the degree of segregation in different points of the simulated environment and can be visualized as maps [12].

The development of the model presented in this work was carried out using the TerraME (Terra Modeling Environment) platform [10]. TerraME is an extended CA-based computational framework for spatial dynamic modeling that implements the concepts of Nested Cellular Automata (Nested-CA). It is an extension of Lua programming language [17], and uses the geoprocessing library TerraLib [9] for handling geospatial data.

2. Methodology

The dynamics of disease dissemination is modeled by a two-dimensional cellular automata grid in which each cell represents an individual. For each time step, each individual can take one of two states: susceptible or infected. To keep the model as simple as possible, births and natural deaths were ignored, as well as incubation periods due to pathogen replication and possible mortality induced by disease.

To investigate the impact of different neighborhood structures on the dynamics of epidemic processes, we performed simulation experiments using two types of neighborhoods. The first one is the classical Moore neighborhood [35], which comprises the eight cells surrounding a central cell (Figure 1(a)). This type of vicinity is used on dissemination processes that depend on contiguous proximity relations, like forest fire propagation [2, 3], cell to cell infection [36] or tumor growth [28]. The second type of neighborhood relies on the concept of activity space, that is, the space in which people live from

day to day, where individuals interact on a daily basis [21]. This is particular important for simulating epidemic processes in which contact relations between individuals are a relevant issue to consider (e.g., respiratory diseases). Therefore, the activity-space neighborhood includes not only relations established in a residential environment, which can be represented by the Moore neighborhood, but also additional ones, such as the relations resulting from work, school and leisure activities. To represent the latter, we added a random component to the neighborhood, as illustrated in Figure 1(b).

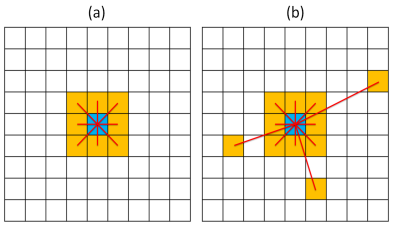

Figure 1. Types of neighborhood: (a) Moore and (b) Activity–space.

For the neighborhoods based on contiguity, we considered the null boundary condition [11], meaning that the cells located on the borders have as neighbors only those cells immediately adjacent to them into the grid. For the random component of the activity-space neighborhood, an average of 2 neighbors for each cell was considered. For that, we considered that each cell of the lattice can be neighbor of a particular cell with probability $2/N^2$, where N^2 is the number of cells in the cellular space.

Initially, the model assumes that a percentage ρ of the population is infected. To test the importance of the spatial distribution of initial disease focus, these early infected individuals were distributed in two ways: concentrated in a central cluster or randomly scattered in the lattice.

Mixing the two types of neighborhood with the two initial spatial distributions of infected people, we performed four experiments based on the following combinations:

Experiment A. Moore neighborhood with a centralized initial disease focus;
Experiment B. Moore neighborhood with initial infected people randomly scattered;
Experiment C. Activity-space neighborhood with a centralized disease focus;
Experiment D. Activity-space neighborhood with initial infected people randomly scattered.

For each time step t, the dynamics of people interactions were based on the following rule: each individual located at position (i, j) can become infected according to the probability

$$Pr(i,j,t) = \beta \cdot \frac{\text{number of infected neighbors of cell } \textit{(i,j)} \text{ at time } t}{\text{number of neighbors of cell } \textit{(i,j)}},$$

where β is the contagion probability. Implicitly, this formula assumes an idea of time-sharing: the more neighbors an individual has, the less time he spends with each neighbor. Figure 2 illustrates some situations of time-sharing. Each circle in Figure 2 represents one individual, while the edges represent the neighborhood relations. The blues circles correspond to susceptible individuals and the red ones represent the infected individuals. In

cases (a) and (b), the individuals at the top of the graph have the same amount of neighbors and, therefore, their chances to get exposed to the pathogen are the same. However, in case (b), the individual at the top is more likely to become infected than the one in case (a). Regarding the case (c), the individual's chance to be exposed to the pathogen is greater than the one in case (a), since the latter has fewer neighbors. However, the individual at the top in case (c) is less likely to become infected than the one in case (a), since he spends less time with each neighbor. The idea of time-sharing is fundamental in our approach, because it differentiates the risk of being exposed to the pathogen from the risk of contracting it.

Figure 2. Some situations of time–sharing. Each circle represents one individual, while the edges represent the neighborhood relations. The blues circles correspond to susceptible individuals and the red ones represent the infected subjects.

Each iteration corresponds to one time step and the common parameters used in all simulations are showed in Table 1.

Table 1. Parameters used in all simulations.

Fixed Parameters	
Dimension of cellular space (N)	51
Percentage of initial infected people (ρ)	0.05
Contagion probability (β)	0.3

For monitoring the simulation outputs, we compute the time needed for achieving the saturation point (all individuals becoming infected) and spatial indices of segregation. In this epidemiological context, indices of segregation are used to depict the potential contact between infected and susceptible individuals. Global and local spatial indices of segregation are calculated: while global indices summarize the segregation degree of the whole city and can be reported and plotted in graphs, local indices depict segregation as a spatially variant phenomenon. The model reports spatial exposure and isolation indices [12]. The global version of the exposure index of group m to n ($exp_{(m,n)}$) measures the average proportion of group n in the neighborhood of each member of group m. The exposure index ranges from 0 to 1 (maximum exposure) and its formula is:

$$exp_{(m,n)} = \sum_{j=1}^{J} \frac{N_{jm}}{N_m} \cdot \frac{L_{jn}}{L_j},$$

where J is the total number of areal units (cells); N_{jm} is the population of group m in areal unit j; N_m is the population of group m in the study area (lattice); L_{jn} is the population belonging to group n in the neighborhood of j; and L_j is the population in the neighborhood of j. The exposure index values depend on the overall population composition of

the study area. For example, if there is an increase in proportion of group n, the value of $exp_{(m,n)}$ tends to become higher. The spatial isolation index ($isol_m$) is a particular case of the exposure index that expresses the exposure of group m to itself. Both indices also present local versions that can be displayed as maps.

3. Results and Discussions

The behavior of the number of infectious individuals (epidemiologically, the prevalence) over the time steps is shown on Figure 3. Each time series evolves under a sigmoidal-like shape (a logistic function): one first region with a fast growth followed by an stationary trend. On the cases with the randomly scattered initial condition, for both neighborhood types (MS and AS curves), the rapid initial growth is explained by the formation of several distinct and simultaneous foci of disease in the first time steps. On the other hand, for both initial condition configurations, the activity-space neighborhood (corresponding to AC and AS curves) is the fastest way of epidemic spreading.

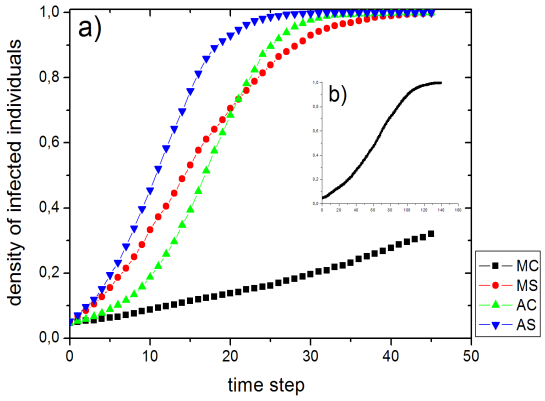

Figure 3. Time series of infected people density. (a) Four time series according with the experiments: MC means Moore neighborhood with concentrated initial infected people; MS means Moore neighborhood with randomly scattered initial infected people; AC means activity-space neighborhood with concentrated initial infected people and AS means activity-space neighborhood with randomly scattered initial infected people. (b) The behavior of MC curve during 139 time steps.

For the four different combinations of neighborhood types and initial spatial distributions, we also compared the dynamics of the density of infected individuals ($densInfec$) with global and local indices of segregation (Figures 4, 5 and 6). The segregation indices considered in the analysis were: isolation of infected individuals ($isolInfec$) and exposure of susceptible to infected individuals ($expSuscInfec$).

In Experiment A, which combines the Moore neighborhood with a centralized initial disease focus, the initial 5% of infected individuals are highly isolated, revealing a global index of isolation of infected individuals of 0.79 (Figure 4(a)). This means that, on average, 79% of the individuals in the surroundings of an infected entity are also infected.

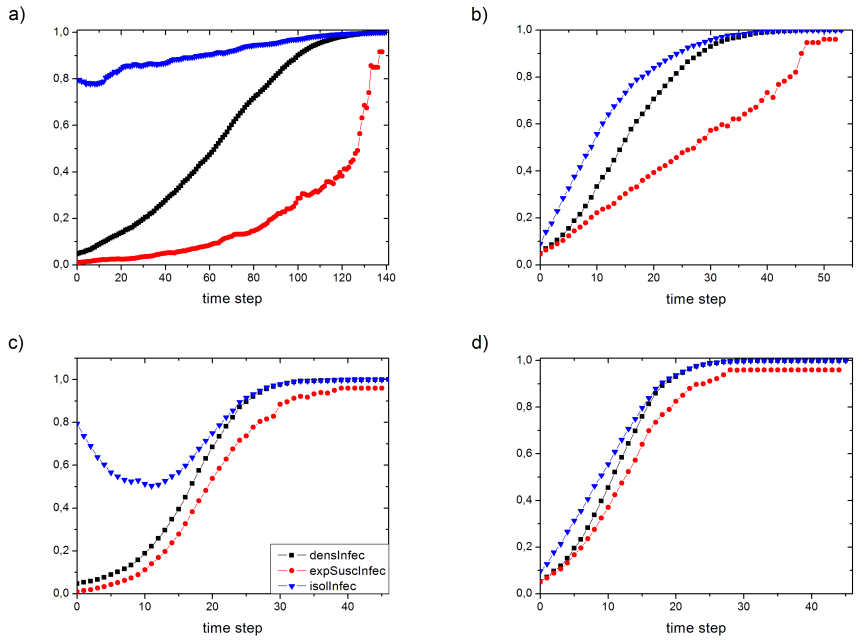

Figure 4. Density of infected individuals ($densInfec$), isolation of infected individuals ($isolInfec$) and exposure of susceptible to infected individuals ($expSuscInfec$) computed for the four experiments based on different combinations of neighborhood types and initial spatial distributions: (a) Moore neighborhood and centralized initial distribution, (b) Moore neighborhood and scattered initial distribution, (c) activity-space neighborhood and centralized initial distribution, and (d) activity-space neighborhood and scattered initial distribution.

On the other hand, the exposure index of susceptible individuals to the infected ones, equal to 0.01, reveals that, on average, only 1% of the individuals in the surroundings of a healthy entity are infected.

The local indices of segregation displayed in Figures 5(a) and 6(a) ($t = 0$) complement this information by showing, respectively, where the infected individuals are initially isolated and the location of a few susceptible individuals with a certain degree of exposure to the infected ones.

As time progresses, the isolation of infected individuals increases slowly, in a linear fashion, and only achieves its maximum value ($isolInfec = 1$) when $t = 139$. It is important to remind that the isolation index necessarily achieves its maximum value at the saturation point, when 100% of the individuals in the surroundings of each infected individual are also infected.

The curve depicting the exposure index of susceptible to infected individuals ($expSuscInfec$) has an exponential-like shape, which increases slowly during the first simulation iterations but accelerates its rhythm as the proportion of infected individuals increases. Figures 5(a) and 6(a) illustrate the spatial pattern of these processes of isolation/exposure, showing how the epidemics dynamics resemble a cluster expansion that

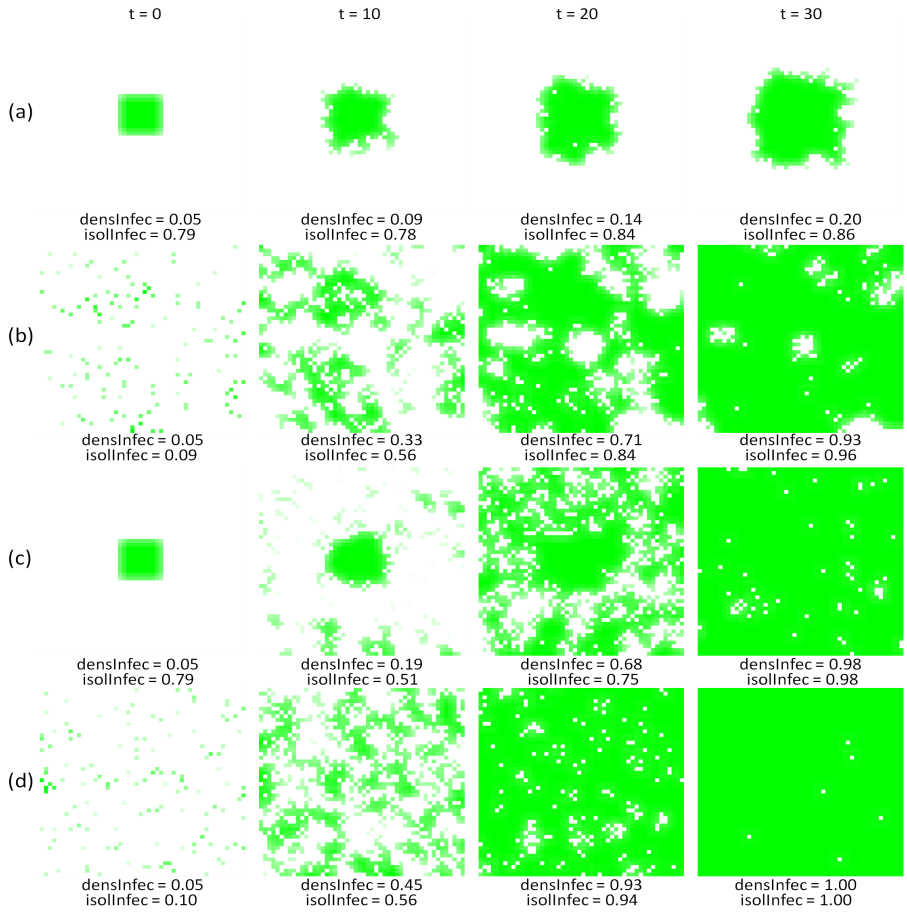

Figure 5. Local indices of isolation of infected individuals computed for four experiments based on different combinations of neighborhood types and initial spatial distributions: (a) Moore neighborhood and centralized initial distribution, (b) Moore neighborhood and scattered initial distribution, (c) activity-space neighborhood and centralized initial distribution, and (d) activity-space neighborhood and scattered initial distribution.

propagates through the lattice. This spreading pattern is consistent for describing processes dictated by contiguous proximity relations.

The Experiment B is similar to the above and also more appropriate to describing dissemination processes ruled by contiguous proximity relations. Nevertheless, in this case, we test the impact of having several initial disease foci randomly scattered in the lattice. Comparing situations A and B in Figure 4, its possible to observe that the scattered initial configuration promoted a strong decrease in the initial isolation of infected individuals ($isolInfec$ decays from 0.79 to 0.09). The exposure of susceptible to infected individuals, on the other hand, increases and reaches the same value as the proportion of infected people ($expSuscInfec = 0.05$), meaning that, on average, a susceptible entity has 5% of infected individuals in its surroundings.

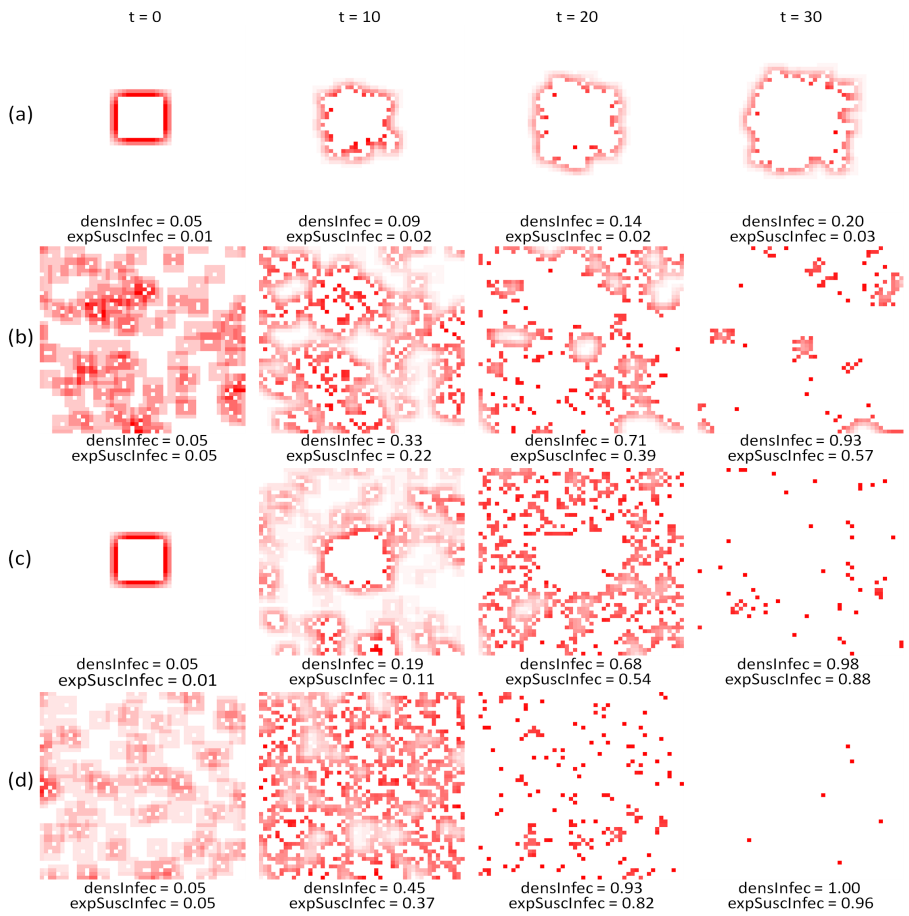

Figure 6. Local indices of exposure of susceptible to infected individuals computed for four experiments based on different combinations of neighborhood types and initial spatial distributions: (a) Moore neighborhood and centralized initial distribution, (b) Moore neighborhood and scattered initial distribution, (c) activity-space neighborhood and centralized initial distribution, and (d) activity-space neighborhood and scattered initial distribution.

Figure 4(b) also shows that the curve describing the isolation index of infected individuals followed a sigmoid shape similar to the one obtained for the density of infected entities. The exposure index of susceptible to infected individuals increased in a linear manner and presents much higher values along the time axis when compared with situation A. In this less-segregated pattern, where the contact between a susceptible and an infected entity becomes more common, it is possible to observe a much faster spread of the epidemics, which saturated at $t = 53$. Figures 5(b) and 6(b) show the local isolation and exposure patterns associated with this type of propagation dynamics.

The Experiment C starts with the same initial condition as the one presented in Experiment A, i.e., with a centralized initial disease focus and a high isolation degree of infected individuals. Nevertheless, it adopts the activity-space neighborhood to model

the interactions between entities, which is a more realistic approach to represent those epidemic processes that depend on direct-contact relations between individuals. Because the activity-space neighborhood includes a non-contiguous component that models those interactions that do not necessarily occur in the surroundings of the individual's residence, the initial isolation of infected individuals strongly decreases during the first iterations of the simulation (Figure 4(c)), when several disease outbreaks appeared (Figure 5(c), $t = 10$) in different points of the lattice. These outbreaks, which are the result of interactions that occur, for instance, during work or school activities, accelerate the dissemination of the epidemic (saturation time equal to 53).

The Experiment D combines the activity-space neighborhood with the initial pattern characterized by several disease foci randomly scattered in the lattice. Comparing with the other experiments, this situation provides the least-segregated patterns between infected and susceptible individuals and, therefore, is also where the saturation point is achieved faster (saturation time equal to 46). Figure 4(d) shows that, in this case, the curves describing the isolation and exposure indices followed the same sigmoid shape as the curve depicting the density of infected individuals. This behavior is the natural trend of both isolation and exposure indices, since an increase in the density of infected individuals also tends to increase the chance of individuals in general (infected or susceptible) to have more infected individuals in their surroundings.

4. Conclusions and Perspectives

This work investigated the effects of neighborhood structures on disease spreading through a compartmental epidemiological CA-model. The paper demonstrated how CA-based models allow the design and exploration of different scenarios of disease transmission dynamics. CA models are able to address the emergence of global spatial patterns of dissemination processes from local interactions between entities and/or individuals. In addition, it provides empirical ways for testing hypotheses and exploring the impacts of public policies.

Considering the concept of neighborhood as an essential aspect to represent interactions between individuals, this work relied on the idea of activity space to explore a neighborhood type that includes not only places surrounding the residential location of individuals, which can be represented by contiguity-based neighborhoods (e.g., Moore), but also additional areas where individuals interact on a daily basis, such as work or school. By combining two types of neighborhood (activity-space or Moore) with two different initial spatial distribution of infected people (centralized or randomly scattered), four different scenarios were simulated and analyzed.

For the analyses, local and global indices of isolation and exposure, normally applied for measuring segregation between social groups, were adopted in this epidemiological context as tools able to depict the spatial arrangement between infected and susceptible individuals as well as the potential contact between them. Using these indices to monitor the simulation scenarios, it was possible to obtain new insights on how epidemics evolve on time and space. The experiments revealed, for instance, how the activity-space neighborhood is related to the appearance of additional disease outbreaks in different areas of the lattice. These outbreaks promote a less-segregated pattern between infected and susceptible individuals and, therefore, a faster spread of the disease.

Such results reinforce the need of considering more realistic neighborhood structures, such as the activity-space neighborhood, to represent epidemic processes that depend on direct-contact relations between individuals. For empirical analysis, the implementation of the activity-space neighborhood would demand the use of additional data that are able to reveal the areas in which people live and interact day-to-day (e.g., origin-destination surveys).

References

[1] Almeida, C. M.; Batty, M.; Monteiro, A. M. V.; Câmara, G.; Soares-Filho, B. S.; Cerqueira, G. C.; Pennachin, C. L. (2003). Stochastic cellular automata modelling of urban land use dynamics: Empirical development and estimation. Computers, Environment and Urban Systems, v. 27, n. 5, p. 481–509.

[2] Almeida, R. M.; Macau, E. E. N. (2011). Stochastic cellular automata model for wildland fire spread dynamics. Journal of Physics. Conference Series (Online), v. 285, p. 012038.

[3] Almeida, R. M. ; Macau, E. E. N. ; França, H. ; Ramos, F. M. ; Carneiro, T. G. S. (2008). Simulando padroes de incendios no Parque Nacional das Emas, Estado de Goias, Brasil. In: X Simpósio Brasileiro de Geoinformática, 2008, Rio de Janeiro - RJ. Anais do X Simpósio Brasileiro de Geoinformática 2008.

[4] Andrade, R. F. S.; Rocha-Neto, I. C.; Santos, L. B. L.; Santana, C. N.; Diniz, M. V. C. et al. (2011). Detecting network communities: An application to phylogenetic analysis. PLoS Computational Biology, v. 7, n. 5. doi:10.1371/journal.pcbi.1001131.

[5] Barker D. P. and Bennett, F. J. (1976). Pratical of epidemiology, Churchill, Livingstone.

[6] Batty, M. (2000). GeoComputation using cellular automata. In: Geocomputation, S. Openshaw and R.J. Abrahart (Eds), New York: Taylor Francis, p. 95–126.

[7] Batty, M.; Xie, Y. (1994). From cells to cities. Environment and Planning B, v. 21, p. 31–48.

[8] Câmara, G. and Monteiro, A. M. V. (2001). Geocomputation techniques for spatial analysis: Are they relevant for health data? Cadernos de Saúde Pública, v. 17, n. 5, p. 1059–1081.

[9] Câmara, G.; Souza, R. C. M.; Pedorsa, B. M.; Vinhas, L.; Monteiro, A. M. V.; Paiva, J. A.; Carvalho, M. T.; Gattass, M. (2000). TerraLib: Technology in support of GIS innovation. II Brazilian Symposium on Geoinformatics, GeoInfo 2000, São Paulo.

[10] Carneiro, T. G. S. (2006). Nested-CA: a foundation for multiscale modeling of land use and land cover change. In: Computer Science Department - INPE, São José dos Campos, SP.

[11] Encinas, L. H.; White, S. H.; Martín del Rey, A.; Sánchez, G. R. (2007). Modelling forest fire spread using hexagonal cellular automata. Applied Mathematical Modelling, v. 31, p. 1213–1227.

[12] Feitosa, F. F.; Câmara, G.; Monteiro, A. M. V.; Koschitzki, T.; Silva, M. P. S. (2007). Global and local spatial indices of urban segregation. International Journal of Geographical Information Science, v. 21, n. 3, p. 299–323.

[13] Góes-Neto, A.; Diniz, M. V. C.; Santos, L. B. L.; Pinho, S. T. R.; Miranda, J. G. V.; et al. (2010). Comparative protein analysis of the chitin metabolic pathway in extant organisms: A complex network approach. BioSystems, v. 101, p. 5966.

[14] Hagoort, M.; Geertman, S; Ottens, H. (2008). Spatial externalities, neighbourhood rules and CA land-use modeling. In: The Annals of Regional Science, v. 42, n. 1.

[15] Hethcote, H. W. (2000). The mathematics of infectious diseases. SIAM Review, vol. 42, n. 4, p. 599-653.

[16] Hill, A. L; Rand, D. G.; Nowak, M. A.; Christakis, N. A. (2010). Infectious disease modeling of social contagion in networks. Plos Computational Biology, v. 6, i. 11.

[17] Ierusalimschy, R.; Figueiredo, L. H. et al. (1996). Lua - an extensible extension language. Software: Practice Experience, v. 26, p. 635–652.

[18] Lana, R.; Carneiro, T. G. S.; Honório, N. A.; Codeço, C. T. (2010). Change allocation in spatially-explicit models for *Aedes aegypti* population dynamics. In: XI Brazilian Symposium on Geoinformatics, GeoInfo 2010, Campos do Jordão.

[19] Martin dél Rey, A.; White, S. H.; Sánchez, G. R. (2006). A model based on cellular automata to simulate epidemic diseases. In: Yacoubi, S. E.; Chopard, B.; Bandini, S. (Eds.): ACRI 2006, LNCS 4173, 304–310. Springer-Verlag Berlin Heidelberg 2006.

[20] Massad E.; Menezes, R. X.; Silveira, P. S. P.; Ortega, N. R. S. (2004). Métodos Quantitativos em Medicina, São Paulo, Editora Manole.

[21] Mayhew, S. (2009). A dictionary of geography. New York: Oxford University Press, 560p.

[22] Medeiros, L. C. C.; Castilho, C. A. R.; Braga, C.; Souza, W. V.; Regis, L.; Monteiro, A. M. V. (2011). Modeling the Dynamic Transmission of Dengue Fever: Investigating Disease Persistence. PLOS neglected tropical diseases. v. 5, n. 1, p. e942. doi:10.1371/journal.pntd.0000942.

[23] Monteiro, A. M. V.; Carvalho, M. S.; Assunção, R.; Vieira, W.; Ribeiro, P. J.; Davis Jr, C.; Regis, L. et al. (2009). SAUDAVEL: Bridging the gap between research and service in public health operational programs by multi-institutional networking development and use of spatial information technology innovative tools. Rev. Bras. Biom., v. 27, n. 4, p. 519–537.

[24] Mikler, A. R.; Venkatachalam, S.; Abbas, K. (2005). Modeling infectious diseases using global stochastic cellular automata. In: Journal of Biological Systems, v. 13, n. 4, p. 421–439.

[25] Mohtashemi, M.; Szolovits, P.; Dunyak, J.; Mandl, K. D. (2006). A susceptible-infected model of early detection of respiratory infection outbreaks on a background of influenza. Journal of Theoretical Biology, v. 241, n. 4, p. 954–963.

[26] Nishiura, H. (2006). Mathematical and statistical analyses of the spread of dengue. Dengue Bull, v. 30, p. 51-67.

[27] Oliveira, G. M. B.; Siqueira, S. R. C. (2006). Parameter characterization of two-dimensional cellular automata rule space. Physica D, v. 217, p. 1-6.

[28] Reis, E. A.; Santos, L. B. L.; Pinho, S. T. R. (2009). A cellular automata model for avascular solid tumor growth under the effect of therapy. Physica A: Statistical Mechanics and its Applications, v. 388, n. 7, p. 1303–1314.

[29] Sarkar, P. (2000). A brief history of cellular automata. ACM Computing Surveys, v. 32, n. 1, p. 80-107.

[30] Santos, L. B. L.; Costa, M. C.; Pinho, S. T. R.; Andrade, R. F. S.; Barreto, F. R.; Teixeira, M. G.; Barreto, M. L. (2009). Periodic forcing in a three-level cellular automata model for a vector-transmitted disease. Physical Review. E, Statistical, Nonlinear, and Soft Matter Physics (Print), v. 80, p. 016102.

[31] Stauffer D.; Sahimi, M. (2007). Can a few fanatics influence the opinion of a large segment of a society? European Physical Journal B, 57: 147-152. DOI: 10.1140/epjb/e2007-00106-7.

[32] Von Neumann, J. (1966). Theory of self-reproducing automata. Illinois: A.W. Burks.

[33] White, S. H.; Rey, A. M.; Sánches, G. R. (2007). Modeling epidemics using cellular automata. Applied Mathematics and Computation, v. 186, p. 193–202.

[34] Wimpenny, J. W.; Colasanti, R. (1997). A unifying hypothesis for the structure of microbial biofilms based on cellular automaton models. FEMS Microbiology Ecology, v. 22, n. 1, p. 1-16.

[35] Wolfram, S. (1994). Cellular Automata and Complexity. New York, Addison-Wesley Publishing Company, p. 316.

[36] Santos, R. M. Z. and Coutinho, S. (2001). Dynamics of HIV infection: A cellular automata approach. Physical Review Letters, v. 87, n. 16. doi:10.1103/PhysRevLett.87.168102.